Diffusion-limited exciton fusion reaction in one-dimensional tetramethylammonium manganese trichloride (TMMC)

Ron Kroon, Hilde Fleurent,* and Rudolf Sprik
Van der Waals–Zeemanlaboratorium, Universiteit van Amsterdam, Valckenierstraat 65, 1018 XE Amsterdam, The Netherlands
(Received 2 November 1992)

We present results of an experimental study on the reaction kinetics of a one-dimensional diffusion-reaction system, on a picosecond to millisecond time scale. Tetramethylammonium manganese trichloride (TMMC) is a perfect model system to study this problem. Time-resolved luminescence of TMMC has been measured over nine decades in time. The nonexponential shape of the luminescence decay curves depends strongly on exciting laser power. This is shown to result from a fusion reaction ($A + A \rightarrow A$) between photogenerated excitons, which is very well described by the diffusion-limited single-species fusion model for initial exciton densities $< 2 \times 10^{-3}$ (fraction of the number of sites). At higher initial exciton densities the diffusion process, and thus the reaction rate, is significantly influenced by the heat produced in the fusion reaction. This is supported by Monte Carlo simulations.

PACS number(s): 05.40.+j, 78.47.+p, 82.20.Mj, 82.40.Js

I. INTRODUCTION

Recent theoretical studies [1–3] have demonstrated the kinetics of diffusion-limited reactions to be determined by the ability of the reaction system to eliminate spatial fluctuations in the concentrations of reactants. Diffusive transport of reactants in three dimensions is well able to eliminate these fluctuations, i.e., to create a spatially uniform concentration of reactants, leading to the well-known classical rate equations to describe the reaction kinetics. However, in systems where diffusive transport is limited to *less* than three dimensions, the classical rate equations are no longer valid. In this case, the diffusing reactants do not explore enough space to eliminate the spatial concentration fluctuations. In fact, the fluctuations grow in time as a consequence of the reactions. This process has been described as a dynamic *self-ordering* of the spatial distribution of reactants [4,5]. The influence of the developing inhomogeneous spatial distribution of reactants on the reaction kinetics is most pronounced in one-dimensional systems.

Up to this date, many theoretical studies have been devoted to this problem [1–7]. In this paper, we present results of a detailed *experimental* study on the dynamics of a diffusion-limited reaction between photogenerated excitons in a one-dimensional system, tetramethylammonium manganese trichloride $(CH_3)_4NMnCl_3$ (TMMC). Where the experimental results are in discrepancy with existing theoretical models, they are analyzed with the aid of Monte Carlo simulations.

We have observed the kinetics of a diffusion-limited reaction between photogenerated excitons in pure TMMC at room temperature by measuring the exciton luminescence decay curves on a picosecond to millisecond time scale, after pulsed laser excitation of the samples. The reaction kinetics is revealed in the excitation power dependence, i.e., the dependence on the initial exciton density, of the nonexponential shape of these curves.

In an earlier study, the TMMC time-resolved luminescence curve was observed to deviate from the exponential form under strong laser excitation [8]. The possibility of a reaction between excitons was indicated, although the excitation power dependence of the luminescence decay curve was not investigated.

In this study we present a thorough investigation of the excitation power dependence of the shape of the TMMC luminescence decay curves. We demonstrate this shape to be governed by a combination of two relaxation channels: (1) a diffusion-limited exciton fusion reaction ($A + A \rightarrow A$) [9] and (2) spontaneous emission. The observed exciton fusion rate on a nanosecond to millisecond time scale accurately identifies one-dimensional diffusion of the excitons to be the rate-limiting process. This is demonstrated by analyzing the luminescence decay curves in terms of the "diffusion-limited single-species fusion model" [4,5]. The model is found to very accurately describe the fusion process over a factor 50 in exciting laser power, up to an initial exciton density of 2×10^{-3} (expressed as a fraction of the number of sites).

At initial exciton densities $> 2\times10^{-3}$ we find a deviation from this model. In this case, the initial reaction rate is observed to rise anomalously fast with increasing laser power. The resulting picosecond luminescence decay, at initial exciton density $\approx 3\times10^{-2}$, was accurately measured using the optical Kerr effect to create a picosecond optical gate. We have analyzed the anomalously fast initial decay of the exciton population using Monte Carlo simulations of the one-dimensional "diffusion-reaction" process, which are to reproduce the experimentally observed picosecond luminescence decay. We show results of simulations of three possible mechanisms that may explain the observed enhancement of the initial reaction rate: (1) an attractive potential between the excitons, (2) a nonlinear absorption process of the optical excitation

pulse which generates excitons on neighbouring lattice sites, and (3) the influence of the heat that is produced upon fusion of two excitons.

The simulations showed the heat produced in the highly exothermic exciton fusion reaction to be responsible for the observed picosecond decay of the exciton population. As a consequence of this heat the diffusion rate of the remaining exciton and, to a lesser extent, other excitons nearby, will be significantly enhanced, causing it to rapidly run into a next exciton. Fusion with this exciton generates more heat, etc. Thus we observe the exothermic reaction to sustain itself, which causes a very rapid decay of the exciton population. Results of the simulations of the other two mechanisms may be applicable to other systems than TMMC.

In the regime of lower exciton density the heat produced in the reactions will be of much less importance, since excitons remaining from a fusion reaction are cooled down to lattice temperature long before they have the chance to meet a new exciton.

This paper is organized as follows: In Sec. II the properties of TMMC are discussed. In Sec. III the theory on the diffusion-limited single-species fusion model is outlined, while the experiment is described in Sec. IV. In Sec. V we present the observed behavior of the luminescence decay curves of TMMC as a function of laser power incident on the samples. Monte Carlo simulations of the one-dimensional diffusion-reaction system are described in Sec. VI. In Sec. VII, results are discussed.

II. PROPERTIES OF TMMC

TMMC, $(CH_3)_4NMnCl_3$, consists of linear chains of face-sharing manganese chloride octahedra (-Mn-Cl_3-Mn-Cl_3-), parallel to the c axis of the crystal [10]. These linear chains are separated by large tetramethylammonium ions, which diminishes the (exchange) interactions between the magnetic Mn^{2+} ions ($S = \frac{5}{2}$) situated on different chains. As a result of the difference in the Mn^{2+} ion separation on the chain (3.25 Å) and between chains (9.15 Å), TMMC behaves as a nearly perfect one-dimensional Heisenberg antiferromagnet [11]. The on-chain exchange interaction exceeds the interchain exchange interaction by four orders of magnitude [11,12].

The chromophore in TMMC is the Mn^{2+} ion. The optical absorption spectrum [11,13,14] is determined by the antiferromagnetic exchange coupling of the Mn^{2+} ion to its nearest neighbors [15]. Excitation of an odd-parity magnon on a neighboring Mn^{2+} ion lifts the spin and parity selection rules of the forbidden single-ion electric dipole transitions.

The localized exciton associated with the lowest excited state of the Mn^{2+} ion exhibits a strong red luminescence ($^4T_{1g} \rightarrow {}^6A_{1g}$ transition), in a broad band centered at 650 nm. Luminescence quenching studies, by doping TMMC samples with low concentrations of transition-metal ions, revealed that the excitons display thermally activated motion along the chain at temperatures larger than 50 K [16]. At room temperature, the on-chain hopping rate in TMMC was found to be 10^{11}–10^{12} s^{-1}, which exceeds the interchain hopping rate by about eight orders of magnitude [17,18]. The energy barrier for on-chain hopping was determined to be 800–1000 cm^{-1} [17], as a result of the lattice distortion created by the exciton.

III. THE DIFFUSION-LIMITED SINGLE-SPECIES FUSION MODEL

The diffusion-limited single-species fusion model [4,5] considers diffusive motion of particles, subject to an irreversible fusion reaction when two particles meet: $A+A \rightarrow A$. In this process, the diffusive transport of the particles constitutes the rate-limiting step. Fusion is assumed to take place instantaneously whenever two particles meet (this is known as the extreme diffusion limit [6]).
At long times and fixed temperature the fusion process obeys the rate equation [4,19]

$$\frac{d\rho(t)}{dt} = -k_T(t)\,\rho^2(t) \quad (t \rightarrow \infty) \tag{1}$$

in which ρ is the particle density and $k_T(t)$, the macroscopic rate "constant" at temperature T, is determined by the dimensionality of the lattice. $k_T(t)$ is related to the microscopic quantity $S(t)$, the random walker's exploration space, i.e., the mean number of distinct lattice sites visited by the random walker [4]: $k_T(t) = [dS(t)/dt]_T$. The expression for $S(t)$ strongly depends on the dimensionality of the lattice [20]. For a one-dimensional lattice $dS(t)/dt \propto t^{-1/2}$. Thus Eq. (1) becomes

$$\frac{d\rho(t)}{dt} = -k_T\,t^{-1/2}\,\rho^2(t), \tag{2}$$

with [6]

$$k_T = \sqrt{\frac{(\Delta x)^2}{\pi\,\tau_{\rm hop}}}, \tag{3}$$

where Δx is the lattice spacing and $\tau_{\rm hop}$ is the average time a particle remains on one site in between two consecutive hops. The general solution of Eq. (2) is [6,2]

$$\frac{\rho(t)}{\rho(0)} = (1 + \alpha\sqrt{t})^{-1}, \tag{4}$$

in which $\rho(0)$ represents the initial exciton density created under pulsed excitation at $t = 0$. In TMMC, the luminescence intensity $I(t)$ is proportional to the instantaneous exciton density $\rho(t)$, since it results from spontaneous radiative decay of the excitons. This allows us to rewrite Eq. (4) as

$$\ln\left(\frac{I(0)}{I(t)} - 1\right) = 0.5\ln(t) + \ln(\alpha), \tag{5}$$

with

$$\alpha = \sqrt{\frac{4}{\pi}}\rho(0)\sqrt{\frac{1}{\tau_{\rm hop}}}. \tag{6}$$

In Eq. (6), the initial exciton density is expressed as a fraction of the number of sites.

The nonclassical rate equation describing the reaction kinetics [cf. Eq. (2)] results from spatial fluctuations in the concentrations of reactants which are not eliminated by the one-dimensional diffusion of the reactants. For the single-species fusion process, this was very well visualized by Kopelman and co-workers [4], and by Ben-Avraham and co-workers [5], who described the time evolution of the distribution of particles on a chain. The starting point is a completely random distribution of particles, characterized by an exponential interparticle distribution function (closest neighbor distance distribution) $p_0(x) = \rho(0)\exp[-\rho(0)\,x]$. As the reaction proceeds, the ensemble of particles exhibits a dynamic *self-ordering* process, characterized by a change of the exponential interparticle distribution function (IPDF) to a skewed Gaussian form $p(x,t) = (\pi/2)\,\rho^2(t)\,x\exp[-(\pi/2)\,\rho^2(t)\,x^2/2]$. The initial reaction rate depends strongly on the exact shape of the initial IPDF. For particles distributed on a chain according to an exponential IPDF the initial reaction rate is 100 times larger than for a skewed Gaussian initial IPDF (at identical initial particle density).

In TMMC, absorption of light from a short optical pulse generates a randomly distributed ensemble of excitons. Starting from an initially random IPDF, Ben-Avraham and co-workers [5] have derived an exact result for the decay of the survival fraction for the $A + A \rightarrow A$ process:

$$\frac{\rho(t)}{\rho(0)} = \left[1 - \mathrm{erf}\left(\sqrt{\frac{\rho^2(0)}{\tau_{\mathrm{hop}}}\,t}\right)\right]\exp\left(\frac{\rho^2(0)}{\tau_{\mathrm{hop}}}\,t\right), \qquad (7)$$

with $\rho(0)$ expressed as a fraction of the number of sites. Comparing the results of Eqs. (4) and (7), one finds them identical within 5% over the time scale of our experiment. Therefore, as will be shown, Eq. (4) is a very good and useful approximation for the interpretation of our experimental results.

IV. EXPERIMENTAL PROCEDURE

To observe the decay of the exciton population in TMMC in time, we have measured the TMMC time-resolved luminescence on a picosecond to millisecond time scale. We have applied the optical Kerr effect [21,22] to create a picosecond optical gate, as shown schematically in Fig. 1.

When an intense linearly polarized light pulse ($\mathbf{E}_2$) travels through an optically isotropic medium, e.g., liquid CS_2, the material becomes temporarily anisotropic. The laserfield $\mathbf{E}_2$ generates a third-order nonlinear polarization inside the medium which results in an induced optical birefringence. In the presence of $\mathbf{E}_2$, the response of the medium to a weak optical signal $\mathbf{E}_1$ will be like that of a uniaxial crystal in which $\mathbf{E}_2$ defines the optic axis. $\mathbf{E}_1$ will experience a polarization rotation, which will be maximum when $\mathbf{E}_1$ is polarized 45° with respect to $\mathbf{E}_2$. $\mathbf{E}_1$ will subsequently pass through polarizer P_2 and be detected. Scanning the position of $\mathbf{E}_2$ in time, with respect to $\mathbf{E}_1$, allows one to measure the transient profile of $\mathbf{E}_1$. In our setup the time resolution is determined by the pulse duration of $\mathbf{E}_2$ [8 ps full width at half maximum (FWHM)], rather than by the damping time of the nonlinear polarization (1.5 ps for CS_2 [23]).

The full setup is shown in Fig. 2. The output of a synchronously pumped dye laser is amplified in a three-stage dye amplifier pumped by the frequency-doubled output of a Q-switched Nd:YAG laser (where YAG denotes yttrium aluminum garnet). The dye amplifier output consists of 1-mJ pulses of 8-ps duration at 580 nm at a repetition rate of 20 Hz. Rhodamine 6G is the active medium in the dye laser, whereas Kiton Red is used in the dye amplifier. Pulse energy is stable within ±8%. Amplified spontaneous emission (ASE) is less than 5 μJ per pulse and is eliminated at the signal frequency by means of a combination of dispersive filtering and dielectric bandpass filters.

A few percent of the beam is split off to monitor pulse energy and pulse shape during the experiment. Subsequently, the beam is split into equal parts. One branch is used to excite the TMMC sample ($^6A_{1g} \rightarrow {}^4T_{1g}$ transition, $\mathbf{E} \perp c$ axis [11,13,14]), the other is used to operate the Kerr gate. The TMMC time-resolved luminescence signal is collected at right angle in a 10-nm bandpass around 660 nm ($^4T_{1g} \rightarrow {}^6A_{1g}$ transition) with a triple-grating spectrometer, and detected with an image-intensified charge-coupled device (ICCD) (Princeton Instruments ICCD-576/SB). The ICCD is gated with a 6.5-ns electronic gate pulse, synchronized to the laser pulse through use of the Nd:YAG laser Q switch as a trigger for the ICCD gate. Stray light at the excitation wavelength is eliminated by a Schott RG630 long-wavelength pass filter.

Use of the electronic ICCD gate is vital to this experiment. Due to the very large ratio of the luminescence lifetime of TMMC ($T_1 = 740\ \mu$s) over the Kerr-gate width (15-ps FWHM), the number of signal photons inside the gate is very small (the peak signal is 75 photons per second impinging on the detector at a Kerr-gate efficiency of 25%). The 10^3 on-off ratio of the optical gate, determined by the quality of the polarizers, requires an effi-

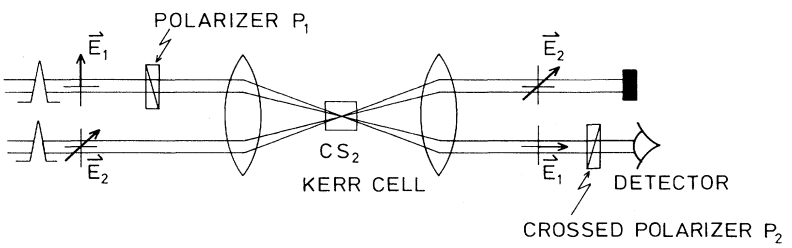

FIG. 1. Schematic showing the principal of the optical Kerr gate. Inside the Kerr medium (CS_2), the strong laser field $\mathbf{E}_2$ induces a polarization rotation of the weak optical signal $\mathbf{E}_1$, allowing it to be detected. A more detailed explanation is given in the text.

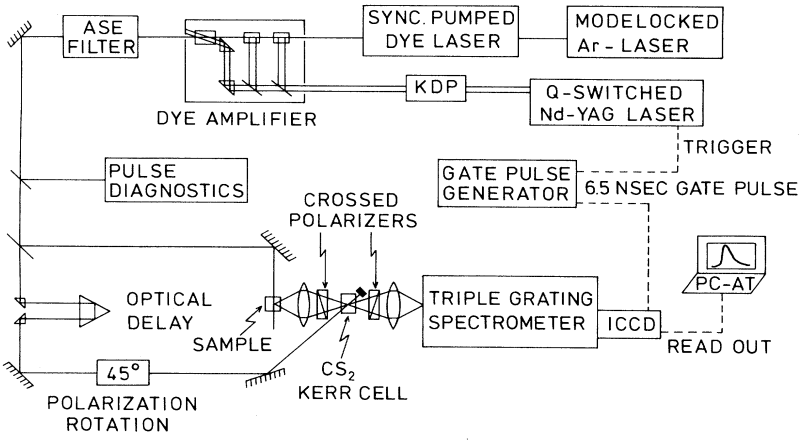

FIG. 2. Picosecond time-resolved luminescence setup, employing the optical Kerr gate. An explanation is given in the text.

cient additional gate to eliminate sample luminescence and photo-cathode dark count at times larger than a few nanoseconds after excitation of the sample. The 10^6 on-off ratio of the ICCD gate proved to be most efficient.

The sensitivity of the setup amounts to ten signal photons per second impinging on the detector. The main source of noise are spurious photons at the signal frequency, generated inside the Kerr cell under the influence of the strong laser beam by a variety of optical processes, such as stimulated Raman scattering, continuum generation, spontaneous Raman scattering, and fluorescence. Integrating over 9000 laser shots renders this background stable within ten photons per second. Time resolution of the setup is less than 5 ps after deconvolution. Time delay was obtained by scanning an optical delay line over a total of 1.5 ns.

Time-resolved luminescence on a nanosecond to millisecond time scale was obtained after pulsed excitation of the TMMC samples with the 532 nm frequency-doubled output of the Q-switched Nd:YAG laser used to pump the dye amplifier in Fig. 2. Pulse duration is 2 ns. The luminescence signal at 660 nm was detected using the ICCD electronic gate to set the time resolution, which is 3 ns after deconvolution. Time delay was obtained by electronically delaying the trigger pulse from the Nd:YAG laser Q switch. Stray light at the excitation wavelength was eliminated by a Schott OG590 long-wavelength pass filter. Signals were reproducible within $\pm 1\%$.

TMMC single crystals were grown from a slightly acidic (10% HCl [11]) aqueous solution containing stoichiometric amounts of $(CH_3)_4NCl$ and $MnCl_2 \cdot 4H_2O$, by slow evaporation at room temperature using a dry nitrogen-gas purge. The crystals grow in bright pink hexagonal rods measuring up to 15 mm in length and 5 mm in diameter. The crystallographic c axis lies parallel to the axis of the rod.

Chemical analysis proved the crystals to be practically free of impurity ions (0.3×10^{-6} mole fraction Cd, 15×10^{-6} mole fraction Cu). The samples were carefully polished using moist lens tissue so as to enhance surface quality and thus damage threshold against laser irradiation. We obtained samples measuring typically $1\times3\times10$ mm^3 with high-quality surfaces. In the experiments, the maximum accessible exciton density did turn out to be limited by laser irradiation-induced sample damage. Results displayed in this paper were obtained below damage threshold. At incident laser-power densities above damage threshold the crystal turned greyish over the entire focal volume.

V. EXPERIMENTAL RESULTS

Time-resolved luminescence of TMMC was measured at room temperature as a function of the exciting Nd:YAG laser power, as shown in Fig. 3. Pulse energies of 0.74–39.9 μJ were focused on a 1-mm-thick sample in a 50- to 70-μm-diam focal spot.

The long-time behavior of the luminescence decay curves is identical, as we derived from measurements extending over a time scale of 10 ms (not shown). It corresponds to an exponential decay with a time constant $T_1 = 740$ μs, which agrees well with the literature values on the population relaxation time of TMMC under weak ex-

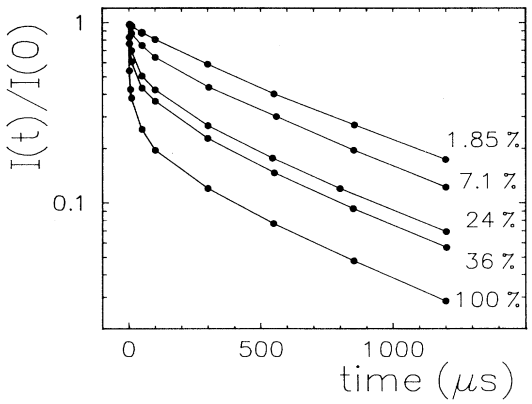

FIG. 3. Logarithmic plot of the experimentally observed TMMC luminescence intensity vs time for various excitation energies. Nd:YAG pulse energies of 0.74–39.9 μJ were incident on the sample. Measurements were taken at room temperature. The curves have been normalized to their values at zero time delay. Solid lines are guides to the eye.

citation conditions [16]. On a sub-millisecond time scale we observe an additional contribution to the decay of the TMMC luminescence signal, which intensifies with increasing laser power.

Further increase of the laser power incident on the sample results in a drastic change of shape of the luminescence decay curves, depicted in Fig. 4. After a fast initial behavior, the decay rate of curves B, C, and D is observed to reduce considerably, leading to a crossing with the 100% curve of Fig. 3, here denoted curve A. At the highest laser powers, the initial decay of the luminescence signal can no longer be resolved by the ICCD gate, as shown in Fig. 4 (inset).

Use of the picosecond optical Kerr gate does reveal the very fast initial luminescence decay behavior for excitation densities comparable to curve F of Fig. 4 (inset). This is shown in Fig. 5. The rise time of the luminescence signal is limited by the instrumental function of the Kerr gate, whereas the signal decays on a time scale of a few hundred picoseconds. The survival fraction at times >1 ns is observed to be significantly lower than the value attained by curve F of Fig. 4 (inset). This is an artifact of the nanosecond ICCD gate: the picosecond decay around zero time delay is underrated with respect to the tail of the luminescence.

When reducing sample temperature to 80 K, under excitation conditions of Fig. 3, exponential decay on a sub-millisecond time scale is obtained, with a decay time $T_1 = 780$ μs (not shown). Its weak dependence on temperature indicates T_1 to be the radiative lifetime of the $^4T_{1g}$ state [16]. Temperature is also found to influence the decay rate for the highest excitation densities, displayed in Fig. 6. As for the weaker excitation conditions of Fig. 3, the decay rate is reduced when lowering temperature, albeit to a much lesser extent. Under the intense laser irradiation, sample temperature in the focus is above 80 K, judging from a slightly nonexponential tail of the low-temperature luminescence decay curve of Fig. 6, on a time scale of 250 μs (not shown).

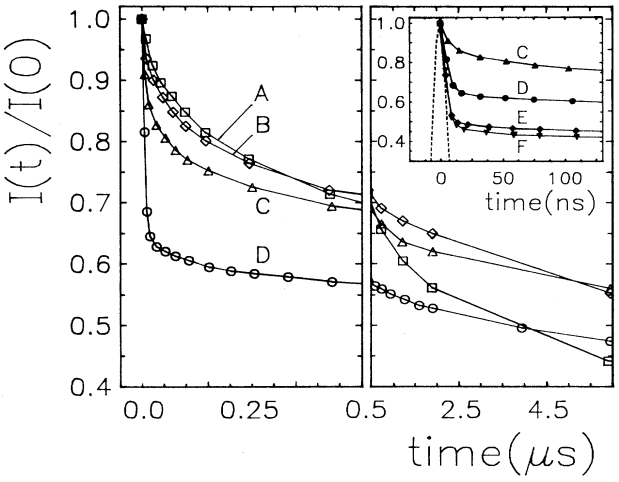

FIG. 4. Decay of the normalized luminescence signal of TMMC. Excitation densities (relative to the 100% curve of Fig. 3) are A, 1.0; B, 2.0; C, 4.1; D, 6.1; E, 8.3; F, 11.2. Measurements were taken at room temperature. Solid lines are guides to the eye. At excitation densities larger than 1.0 the decay curves change shape, with respect to Fig. 3. Inset: For high excitation densities the initial decay is unresolved by the ICCD gate. The dashed line shows the instrumental function of the ICCD gate.

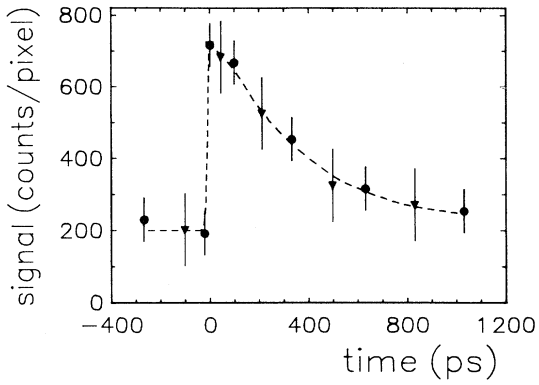

FIG. 5. Picosecond time-resolved luminescence signal of TMMC at high initial exciton density [in the order of a percent of the number of sites, comparable to curve F of Fig. 4 (inset)], obtained using the optical Kerr gate. The results of two measurements are shown. The dashed line is a guide to the eye.

VI. MONTE CARLO SIMULATIONS

As we will show in Sec. VII, the experimental results of Figs. 4 and 5 are not described by the single-species fusion model. To analyze these experimental results, we have simulated the diffusion-limited $A + A \rightarrow A$ reaction on a one-dimensional lattice via the Monte Carlo tech-

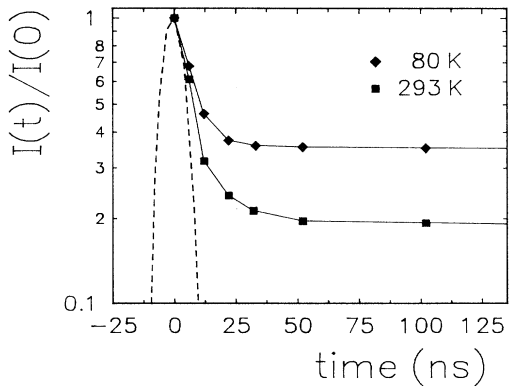

FIG. 6. The effect of temperature on the behavior of the normalized TMMC luminescence intensity in time, at high initial exciton density (in the order of a percent). Data have been taken at 293 K (diamonds) and 80 K (boxes). Solid lines are guides to the eye. The dashed line shows the instrumental function of the ICCD gate.

nique, which simulates the actual motion and reaction of the particles.

We first distribute the initial particles on the chain, one by one, displaced from each other at a random distance determined by the exponential interparticle distribution function. Then, one by one, we allow the particles to hop, i.e., the particle is shifted to one of its two neighboring sites with equal probabilities (this simulates the diffusive motion of the particles). For the hopping particle we draw a random number from the (exponential [24]) waiting-time distribution for hopping, which has the hopping time as the average. The particle's waiting time thus obtained, between its current hop and its one before that, is added to its survival time, which describes how long the particle survives in the diffusion-reaction system (this simulates the hopping of particles to take place at random moments).

At the completion of a hop, we check for fusion of two particles. If the target site is already occupied by another particle, then one of the two particles is removed from the chain at random, decreasing the total number of particles by one.

The survival-time distribution is the negative time derivative of the particle density $\rho(t)$, i.e., it describes the number of reacting particles in time. Thus, from the survival-time distribution one directly calculates the survival fraction $\rho(t)/\rho(0)$. Statistics of the survival-time distribution, the survival fraction, and the interparticle distribution function are taken at various times during a run. We use chains that contain 500 particles, with periodic spatial boundary conditions. We then average over 500 chains, in order to ensure proper statistics.

The simulation procedure as outlined above does yield results which are described by the single-species fusion model. The experimentally observed deviation from this model at high initial exciton densities is simulated by incorporating into this procedure several mechanisms that influence the diffusion-reaction process, such as a potential between the excitons. Results will be shown in Sec. VII. To treat this problem we have refrained from an analytical approach, since that would be very difficult to solve.

VII. DISCUSSION

Experimental evidence for the occurrence of an exciton annihilation or fusion reaction [9] in TMMC is presented in Fig. 7, where we plot the total luminescence signal [i.e., $I(t)$ integrated over time] of Fig. 3 versus Nd:YAG laser pulse energy incident on the sample. In the absence of exciton annihilation or fusion one should observe the experimental data to follow the dashed line. We clearly observe loss of signal at 660 nm (our wavelength of detection).

Exciton annihilation processes have been thoroughly studied in molecular crystals like anthracene [25]. There, two triplet excitons often annihilate to form a singlet exciton at approximately twice the triplet exciton energy. The presence of the singlet exciton can be traced by its luminescence, so-called delayed luminescence [26]. This reaction consumes two excitons: $A + A \rightarrow \hbar\omega$.

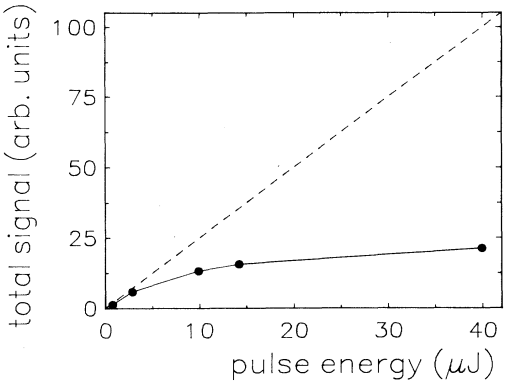

FIG. 7. Integral of the experimentally observed TMMC luminescence signal $I(t)$ of Fig. 3 over time, plotted vs excitation energy incident on the sample. In the absence of exciton annihilation or fusion one should observe the experimental data to follow the dashed line.

In TMMC no delayed fluorescence has been observed: the $^4T_{1g} \rightarrow {}^6A_{1g}$ transition is the only emission band of TMMC [8,11,16]. The observed signal loss at 660 nm therefore cannot be ascribed to an annihilation-induced radiative decay mechanism.

A likely scenario for *nonradiative* loss of excitons in TMMC considers two excitons meeting on a single lattice site, thus exciting the Mn^{2+} ion to twice the exciton energy. Subsequently, emission of phonons causes the ion to relax back to the $^4T_{1g}$ state. This reaction consumes one exciton: $A + A \rightarrow A$+heat. An exciton-fusion mechanism similar to that described here has been observed by Diggle, Gehring, and Mcfarlane [27] for excitons in $TbPO_4$, and was used by Wilson, Hegarty, and Yen [28] to explain biexciton decay in MnF_2.

Exciton fusion in TMMC is found to cease upon lowering sample temperature to 80 K under excitation conditions of Fig. 3 (at 80 K we obtain exponential luminescence decay curves). Thus it is obvious that the transport properties of the excitons play a crucial role in the fusion process.

The nonexponential behavior of the luminescence decay curves of Fig. 3 is favorably described by the diffusion-limited single-species fusion model. This is shown in Fig. 8(a) where the curves are reproduced corresponding to the form of Eq. (5). The observed linear dependence with slope 0.5 (cf. Table I) accurately identifies the one-dimensional character of the exciton fusion process in TMMC under sufficiently strong laser excitation. For laser pulse energies of 14.2 and 39.9 μJ (the 36% and 100% curves of Fig. 3) we are able to follow the exciton diffusion-fusion kinetics over four decades in time. At times ≥ 100 μs we observe the influence of spontaneous emission as a deviation from linear behavior in Fig. 8(a).

The best linear least-squares fit parameters to Eq. (5), represented by the solid lines in Fig. 8(a), are listed in Table I. We follow Eq. (6) to calculate the values for the initial exciton density $\rho(0)$ from the α values obtained from the fits. The values for $\rho(0)$ thus obtained are plot-

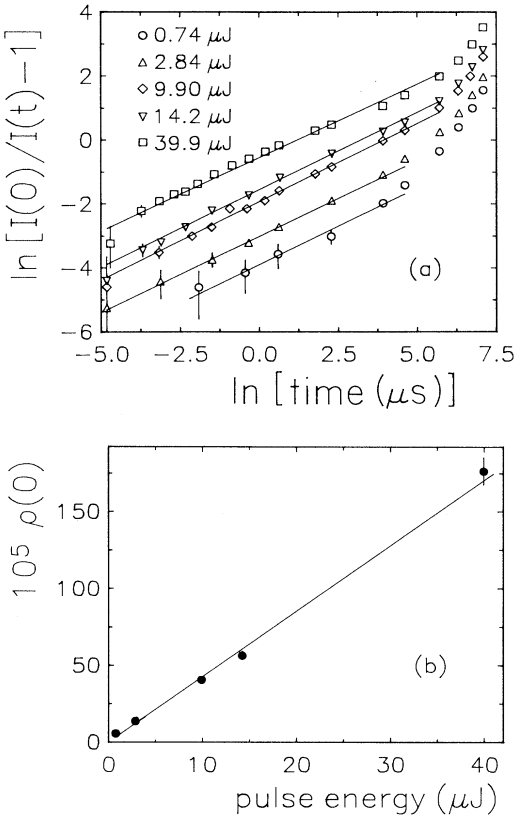

FIG. 8. Analysis of the TMMC luminescence decay curves of Fig. 3 in terms of the diffusion-limited single-species fusion model. (a) Double logarithmic plot of the luminescence decay curves. Solid lines are best fits to Eq. (5). Exciting Nd:YAG pulse energies are indicated. (b) Initial exciton density $\rho(0)$ vs laser pulse energy incident on TMMC, derived from Eq. (6). The solid line is a guide to the eye. $\rho(0)$ is expressed as a fraction of the number of sites. See also Table I.

ted versus laser pulse energy incident on the sample in Fig. 8(b). The linear scaling of $\rho(0)$ with incident laser energy confirms the adequacy of the theoretical model. For the calculation of $\rho(0)$, in Eq. (6) a hopping time of 10 ps was used [17,18]. The initial exciton density derived from the experimental excitation conditions (input laser power, interaction volume, and TMMC absorbance at 532 nm [16]) is in accordance with the $\rho(0)$ values of Table I.

TABLE I. Initial exciton density $\rho(0)$ vs Nd:YAG laser pulse energy incident on the TMMC sample. The slope and parameter α of the solid lines in Fig. 8(a) are derived by fitting the experimentally observed luminescence decay curves of Fig. 3 to Eq. (5). Corresponding values for $\rho(0)$ are derived from Eq. (6) with $\tau_{hop} = 10$ ps. $\rho(0)$ is expressed as a fraction of the number of sites.

Pulse energy (μJ)	Slope	α	$\rho(0)$
0.74	0.480	0.020	5.66×10^{-5}
2.84	0.475	0.049	1.37×10^{-4}
9.90	0.495	0.145	4.07×10^{-4}
14.23	0.485	0.202	5.66×10^{-4}
39.93	0.460	0.625	1.77×10^{-3}

A drastic change in the shape of the luminescence decay curves results from increasing the laser power on the TMMC samples beyond the 100% curve of Fig. 3. This is shown in Fig. 4. In this case, the initial decay rate is considerably higher than predicted by the diffusion-limited single-species fusion model, after which the decay rate is observed to reduce substantially. Decay following the diffusion-limited single-species fusion model appears at later times. For curves B and C this happens ≈ 250 ns after excitation, for curves D, E, and F, ≈ 70 ns after excitation. Concerning the latter curves, the total signal emitted within 100 ns after excitation increases linearly with laser power. This may be due to the onset of a steady state between exciton decay and input of excitons by absorption of light from the Nd:YAG pulse [5].

In the following we will discuss the origin of the observed anomalous enhancement of the initial luminescence decay rate for incident laser powers beyond the 100% curve of Fig. 3. We will first show that this effect is not the result of the onset of a new population-relaxation channel like ASE in the TMMC sample, but that also in this regime of high incident laser pulse energy the diffusion-limited exciton-fusion process constitutes the dominant decay channel. We will then consider three mechanisms that may explain the observed enhancement of the initial reaction rate. These possible mechanisms are analyzed in Monte Carlo simulations of the one-dimensional diffusion-reaction process, which are to reproduce the picosecond luminescence decay observed with the optical Kerr gate (cf. Fig. 5). The very rapid enhancement of the initial luminescence decay rate with increasing laser power that is shown in Fig. 4 indicates that the influence of the proposed mechanisms should scale highly nonlinearly with initial exciton density. In the Monte Carlo simulations, we have therefore analyzed the following mechanisms: (1) an attractive potential between the excitons, (2) a nonlinear absorption process of the optical excitation pulse which generates excitons on neighboring lattice sites, and (3) the influence of the heat that is produced upon fusion of two excitons. It will be shown that the third mechanism is responsible for the observed anomalous enhancement of the initial decay rate. Results of the simulations of the other two mechanisms may be applicable to other systems than TMMC.

The very fast initial luminescence decay cannot be ascribed to ASE in the TMMC sample because of the very low cross section for stimulated emission of the ${}^4T_{1g} \rightarrow {}^6A_{1g}$ transition. For a four-level system with a Gaussian emission band, as is approximately the case for TMMC [16], with a band center $\lambda_{max} = 650$ nm, bandwidth $\delta\nu = 2000$ cm^{-1} (FWHM), radiative lifetime $T_1 = 740$ μs, and a refractive index $n = 1.588$ [10], the transition cross section is calculated to be $\sigma = \sqrt{\ln(2)}\,\lambda_{max}^2\,(4\pi^{3/2}\,n^2\,T_1\,\delta\nu)^{-1} = 1.41\times10^{-21}$ cm^2 [29,30], which is to be compared to 3×10^{-16} cm^2 for an organic laser dye (Rhodamine 6G). Concerning our experimental conditions (sample thickness $L = 1$ mm; focal diameter $d = 50$ μm; incident

Nd:YAG pulse energy corresponding to curve F of Fig. 4, 450 μJ; absorbance at 532 nm, 3 cm^{-1}), this results in a power amplification coefficient $2\alpha_m = N\sigma = 0.21$ cm^{-1}, in which N is the inversion population density [29]. Finally, we calculate the ratio of the amplified spontaneous-emission rate to the purely spontaneous-emission rate for our interaction volume to be $(d/4L)^2(e^{2\alpha_m L} - 1) = 3.3\times10^{-6}$ [29, p. 552]. Thus, in TMMC purely spontaneous emission is highly dominant over amplified spontaneous emission.

Experimental indication that we cannot ascribe the initial luminescence decay to ASE is displayed in Fig. 6, where we observe a reduced decay rate at lower temperature. The cross section of the $^4T_{1g}\rightarrow{}^6A_{1g}$ transition increases by 10% when reducing temperature to 80 K [14,16]. The concept of ASE can therefore not explain the observed reduction in the luminescence decay rate. A second indication is in the number of signal photons inside the Kerr gate (gate width $\delta t_{\rm Kerr}$) at zero time delay. Taking into account our signal collection efficiency, and the exciton population N, created by the picosecond optical pulse, the number of signal photons is equal to $N\delta t_{\rm Kerr}/T_1$, i.e., it results from purely spontaneous emission. The observed temperature dependence of the luminescence decay rate and the measured signal inside the Kerr gate imply that also in this high-exciton-density regime the observed luminescence decay is the result of the fusion of excitons.

The behavior of the luminescence decay curves of Fig. 4 implies that the excitons very rapidly attain an "ordered" interparticle distribution function. As a result, at longer times their decay rate will be considerably reduced. We will now analyze the possible mechanisms that may explain the anomalously fast attainment of an ordered distribution. The results of the Monte Carlo simulations are compared to the experimental data obtained with the optical Kerr gate. We will first discuss the physical origin of the attractive potential between the excitons in TMMC.

The exciton in TMMC exhibits a strong coupling to phonons, as inferred from the high-energy barrier for hopping (800–1000 cm^{-1} [17]). This results in self-trapping [31] of the exciton by the lattice distortion that it creates, i.e., it is a small exciton polaron. The deformation field allows the exciton polarons to mutually interact, leading to a net attractive potential. This is a well-described phenomenon for electron polarons [32,33]. The potential will lead to a reduced randomness in the motion of the excitons. Excitons close to each other will display a preference to hop towards each other (and subsequently react).

We have simulated an attractive potential between the excitons by reducing the energy barrier for hopping, expressed as a reduced hopping time, in a preferred direction. Results of simulations are shown in Fig. 9. We have used an exponential potential $V(x) = V(0)\exp(-x/b)$, with the distance between excitons x expressed in units of lattice parameter. The energy barrier for hopping (taken to be 1000 cm^{-1}, i.e., 1439 K) was chosen to be the order of magnitude of $V(0)$. We have applied an initial exciton density $\rho(0) = 5\%$, and a hopping time (of a particle alone on a chain) $\tau_{\rm hop} = 10$ ps.

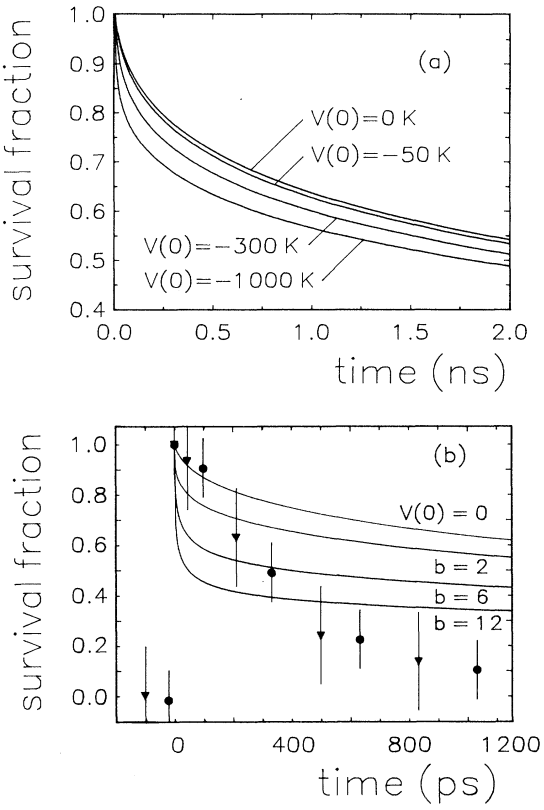

FIG. 9. Monte Carlo results showing the effect of an attractive potential between the exciton polarons, $V(x) = V(0)\exp(-x/b)$, on the diffusion-limited $A + A \rightarrow A$ reaction in one dimension. $\rho(0) = 5\%$, $\tau_{\rm hop} = 10$ ps. (a) The survival fraction as a function of $V(0)$ with $b = 2$. (b) The survival fraction as a function of b with $V(0) = -1000$ K. It is seen that the shape of the simulated curves does not match the experimental result.

The attractive potential induces a strong enhancement of the initial reaction rate, both as a function of potential strength $V(0)$ [cf. Fig. 9(a)] and as a function of the range of interaction b [cf. Fig. 9(b)]. It is seen, however, that the notion of an attractive potential does not explain the results obtained in the picosecond experiment. The shape of the simulated decay curve is actually opposite to the experimental result. The initial decay is too fast, the subsequent decay is too slow. Several other potentials [$V(x) \propto x^{-1}$, x^{-3}] yielded similar results.

A second possibility to rapidly attain an ordered IPDF lies in a change in the nature of the optical-absorption process at high laser-power densities, i.e., the onset of a nonlinear absorption process in which two visible photons are absorbed under creation of two excitons at neighboring sites. Since the two excitons are created at different sublattices, the spin selection rule is fulfilled [34]. In the simulations, when distributing the initial particles on the chain, a random number is drawn to decide between placing one particle, or two neigboring particles. The nonlinear absorption process results in an IPDF that has the exponential form with a high peak superimposed

at an interexciton distance of one lattice parameter. In the simulations, the survival fraction is found to decay qualitatively similar to the use of an attractive potential. Therefore, also the concept of nonlinear absorption of light does not explain the experimentally observed picosecond decay of the exciton population.

So far, we have considered the ideal case, $A + A \rightarrow A$, without taking into account the by-product of the fusion reaction: heat. With every reaction, 1.9 eV (22 000 K) is released in the form of phonons. The exciton that remains from the reaction is in the midst of this "shower" and will feel its influence, aided by the strong exciton-phonon coupling. Experiment indicates that heating due to fusion should be taken into account. When cooling the sample to 80 K, we observe only a moderate reduction of the reaction rate at high input laser power (cf. Fig. 6), in contrast to the behavior at the weaker excitation conditions of Fig. 3. Also, in the experiments the maximum accessible exciton density proved limited by laser irradiation induced sample damage. This shows fusion induced heating to be quite a drastic effect, since we have determined the (lattice) temperature at which TMMC dissociates to be 368 °C.

Effects of heating are simulated, in an empirical manner, by assigning an exciton that remains of a fusion reaction a higher temperature ($T^*_{\rm exc}$), i.e., a reduced hopping time. The "hot" excitons are assumed to react before loosing their temperature, on account of the high density of excitons and the strong exciton-phonon coupling. The energy barrier for hopping (1000 $\rm cm^{-1}$, i.e., 1439 K) was chosen to be the order of magnitude of $T^*_{\rm exc}$. Results of the simulations are shown in Fig. 10.

In Fig. 10(a), the behavior of the simulated survival fraction is seen to approximate the shape of the experimental data. Monte Carlo results for two values of the hopping time are shown, in view of the experimental uncertainty regarding its value [17,18]. Values for $\rho(0)$ are chosen to fit the experimental result. Their order of magnitude is in accordance with the value derived from the experimental excitation conditions ($\approx$3%). The effect of the temperature that we assign the hot excitons is found to rapidly saturate; cf. Fig. 10(b). However, the heat that is produced in the reactions will also influence excitons which, at that moment, do not participate in a reaction. This process is effective in three dimensions (in TMMC at room temperature there is no anisotropy in the heat conductivity [35]). It has been simulated in Fig. 10(c), where we have raised the average temperature proportional to the reaction rate: every ten reactions the average temperature was raised by 5 K.

The heating process is observed to be most influential, not so much in the initial stage of the reaction process, but more in the subsequent stage. This follows from the nature of the process. The enhanced hopping rate of the excitons that results from the heat produced in the reactions brings about an increase of the reaction rate, which results in more heat being produced, etc. The reaction sustains itself.

The present Monte Carlo simulations represent a semi-empirical method to qualitatively understand our experimental results. A calculation that takes into account the effects of exciton-phonon coupling on the (three dimensional) heating and cooling of all excitons on a first-principles basis is required to quantitatively explain the fusion process that takes place in TMMC.

The diffusion-reaction process in TMMC may be influenced by the exchange interaction between the exci-

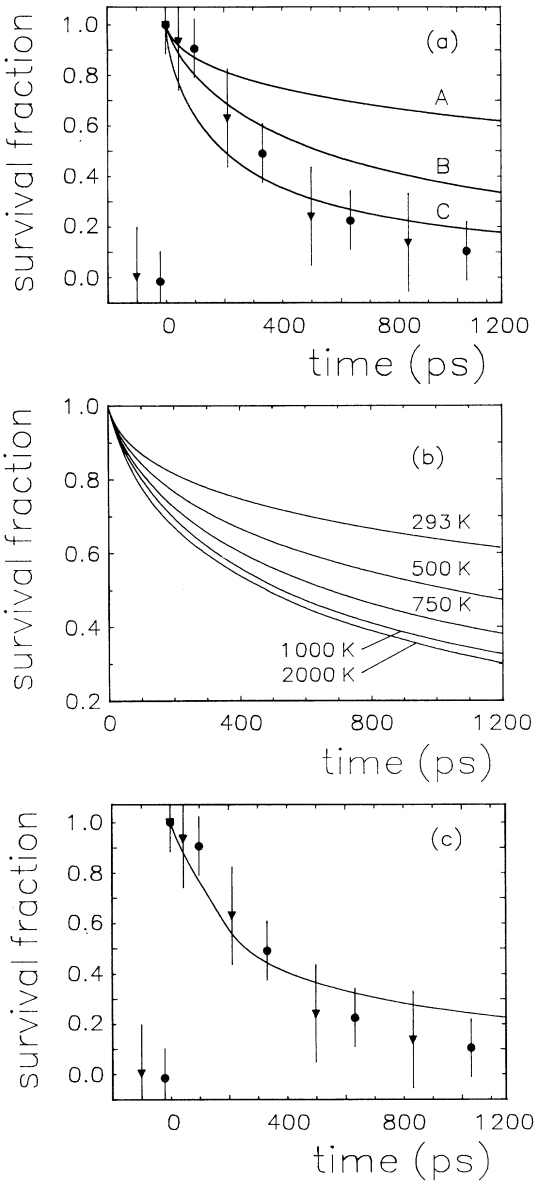

FIG. 10. Monte Carlo simulations show the influence of heat produced in the fusion reaction on the decay of the exciton population. (a) A: $T^*_{\rm exc}$ = 293 K (no heating), $\rho(0)$ = 5%, $\tau_{\rm hop}$ = 10 ps; B: $T^*_{\rm exc}$ = 1000 K, $\rho(0)$ = 5%, $\tau_{\rm hop}$ = 10 ps; C: $T^*_{\rm exc}$ = 1000 K, $\rho(0)$ = 2.5%, $\tau_{\rm hop}$ = 1 ps. (b) The effect of $T^*_{\rm exc}$ rapidly saturates. Assigned $T^*_{\rm exc}$ is indicated. $\rho(0)$ = 5%, $\tau_{\rm hop}$ = 10 ps. (c) We have included heating of the lattice proportional to the reaction rate, as described in the text. $T^*_{\rm exc}$ = 1000 K, $\rho(0)$ = 5%, $\tau_{\rm hop}$ = 10 ps. The shape of the simulated curve is seen to match the experimental result very well.

tons [36]. When situated on neighboring sites, excitons with parallel spins repel each other while those with opposite spins attract each other. We have simulated the effect of this interaction. The strength of the interaction is taken to be $V_{nn} = \pm 50$ K, where the sign depends on the spin of the excitons. This value is slightly higher than the 31.5-K exchange interaction between ground-state Mn^{2+} ions [11,37], on account of the larger spatial extent of the excited state. In the Monte Carlo results, the presence of the exchange interaction is hardly observable. It does not influence the decay of the exciton population within 0.25%. Therefore, in all Monte Carlo simulations presented here, we have neglected the exchange interaction between the excitons.

Results of our Monte Carlo simulations demonstrate the initial reaction rate to be strongly influenced by the reaction probability (when two particles meet they fuse with probability η, where $\eta \leq 1$, and pass through each other with probability $1 - \eta$). In view of the highly efficient reaction process observed in the experiments, reaction probability was assumed to be one in all Monte Carlo simulations presented here. The reaction probability is determined by the ratio of the reaction time to the hopping time. The reaction time is expected to be of the order of the time of formation of the excitons (the relaxation time of the lattice to a distortion), which is equal to the reciprocal of the phonon bandwidth, i.e., ≈ 100 fs. The reaction time will thus be much shorter than the hopping time, hence our interpretation of the data in terms of the extreme diffusion limit. The short time of formation of the excitons also explains the observed rise time in the picosecond Kerr gating experiment (cf. Fig. 5) to be limited to the rise time of the instrumental response function.

In summary, we have studied the dynamics of a diffusion-reaction system in one dimension, on a picosecond to millisecond time scale. Photogenerated excitons in tetramethylammonium manganese trichloride (TMMC) are found to exhibit a fusion reaction ($A+A \rightarrow A$+heat), rate limited by one-dimensional diffusion. At initial exciton densities $<2\times10^{-3}$ (fraction of the number of sites), the reaction process is well described by the diffusion-limited single-species fusion model. At higher initial exciton densities, the heat produced in the fusion reaction significantly enhances the diffusion rate of the reactants, and thus the reaction rate.

ACKNOWLEDGMENTS

We would like to express our gratitude to Ad Lagendijk, Yu. M. Kagan, and G.V. Shlyapnikov for stimulating discussions. Excellent experimental assistance by Wim Koops, M.M. Groeneveld, J. Kragten, and Gjalt Feenstra is also highly appreciated. This research has been supported by the Stichting voor Fundamenteel Onderzoek der Materie (FOM), which is financially supported by the Nederlandse Organisatie voor Wetenschappelijk Onderzoek (NWO).

* Present address: Laboratoire Aimé Cotton, Université Paris Sud, Bâtiment 505, 91405 Orsay CEDEX, France.

[1] D. Toussaint and F. Wilczek, J. Chem. Phys. **78**, 2642 (1983).
[2] G. Zumofen, A. Blumen, and J. Klafter, J. Chem. Phys. **82**, 3198 (1985).
[3] K. Kang and S. Redner, Phys. Rev. A **32**, 435 (1985).
[4] R. Kopelman, Science **241**, 1620 (1988); J. Stat. Phys. **42**, 185 (1986); R. Kopelman, S.J. Parus, and J. Prasad, Chem. Phys. **128**, 209 (1988).
[5] D. Ben-Avraham, M.A. Burschka, and C.R. Doering, J. Stat. Phys. **60**, 695 (1990); C.R. Doering and D. Ben-Avraham, Phys. Rev. A **38**, 3035 (1988).
[6] D.C. Torney and H.M. McConnell, J. Phys. Chem. **87**, 1941 (1983).
[7] L.W. Anacker and R. Kopelman, J. Chem. Phys. **81**, 6402 (1984); Phys. Rev. Lett. **58**, 289 (1987); K. Lindenberg, B.J. West, and R. Kopelman, *ibid.* **60**, 1777 (1988); C.R. Doering and D. Ben-Avraham, *ibid.* **62**, 2563 (1989); M.A. Burschka, C.R. Doering, and D. Ben-Avraham, *ibid.* **63**, 700 (1989); C.R. Doering and M.A. Burschka, *ibid.* **64**, 245 (1990); D. Ben-Avraham and C.R. Doering, Phys. Rev. A **37**, 5007 (1988); J.C. Lin, *ibid.* **43**, 5714 (1991); **45**, 3892 (1992); I.M. Sokolov, H. Schnörer, and A. Blumen, *ibid.* **44**, 2388 (1991); Z. Racz, Phys. Rev. Lett. **55**, 1707 (1985); J.L. Spouge, *ibid.* **60**, 871 (1988); M. Bramson and J.C. Lebowitz, *ibid.* **61**, 2397 (1988); V. Kuzovkov and E. Kotomin, Rep. Prog. Phys. **51**, 1479 (1988).
[8] R.L. Blakley, C.E. Martinez, M.F. Herman, and G.L. McPherson, Chem. Phys. **146**, 373 (1990).
[9] We use the following nomenclature: The reaction $A + A \rightarrow A$ is named a *fusion* reaction, in contrast to $A + A \rightarrow$inert, which we call an *annihilation* reaction.
[10] B. Morosin and E.J. Graeber, Acta Crystallogr. Sec. A **23**, 766 (1967).
[11] R. Dingle, M.E. Lines, and S.L. Holt, Phys. Rev. **187**, 643 (1969).
[12] M. Steiner, J. Villain, and C.G. Windsor, Adv. Phys. **25**, 87 (1976).
[13] K.E. Lawson, J. Chem. Phys. **47**, 3627 (1967).
[14] P. Day and L. Dubicki, J. Chem. Soc. Faraday Trans. II **69**, 363 (1973).
[15] L.L. Lohr and D.S. McClure, J. Chem. Phys. **49**, 3516 (1968).
[16] H. Yamamoto, D.S. McClure, C. Marzzacco, and M. Waldman, Chem. Phys. **22**, 79 (1977).
[17] R.A. Auerbach and G.L. McPherson, Phys. Rev. B **33**, 6815 (1986).
[18] R. Knochenmuss and H.U. Güdel, J. Chem. Phys. **86**, 1104 (1987).
[19] R.M. Noyes, Prog. React. Kinet. **1**, 128 (1961).
[20] E.W. Montroll and G.H. Weiss, J. Math. Phys. **6**, 167 (1965).
[21] M.A. Duguay and J.W. Hansen, Opt. Commun. **1**, 254 (1969).
[22] P.P. Ho and R.R. Alfano, Phys. Rev. A **20**, 2170 (1979).
[23] B.I. Greene and R.C. Farrow, Chem. Phys. Lett. **98**, 273

(1983).
[24] W.H. Press, B.P. Flannery, S.A. Teukolsky, and W.T. Vetterling, *Numerical Recipes* (Cambridge University Press, Cambridge, 1986).
[25] For a comprehensive review see K.C. Kao and W. Hwang, *Electrical Transport in Solids* (Pergamon, Oxford, 1981).
[26] R.G. Kepler, J.C. Caris, P. Avakian, and E. Abramson, Phys. Rev. Lett. **10**, 400 (1963).
[27] P.C. Diggle, K.A. Gehring, and R.M. Mcfarlane, Solid State Commun. **18**, 391 (1976).
[28] B.A. Wilson, J. Hegarty, and W.M. Yen, Phys. Rev. Lett. **41**, 268 (1978).
[29] A.E. Siegman, *Lasers* (University Science Books, Mill Valley, CA, 1986).
[30] L.F. Mollenauer, in *Laser Handbook, Vol. 4*, edited by M.L. Stitch and M. Bass (North-Holland, Amsterdam, 1985).
[31] Y. Toyozawa, in *Relaxation of Elementary Excitations*, Proceedings of the Taniguchi International Symposium, Susono-shi, Japan, edited by R. Kubo and E. Hanamura (Springer-Verlag, Berlin, 1980).
[32] H. Hiramoto and Y. Toyozawa, J. Phys. Soc. Jpn. **54**, 245 (1985).
[33] H. De Raedt and A. Lagendijk, Z. Phys. B **65**, 43 (1986).
[34] R. Moncorgé and B. Jacquier, in *Collective Excitations in Solids*, Proceedings of the NATO Advanced Studies Institute on Collective Excitations in Solids, Enrice, Italy, edited by B. Di Bartolo and J. Danko (Plenum, New York, 1983).
[35] H. Miike and K. Hirakawa, J. Phys. Soc. Jpn. **39**, 1133 (1975).
[36] E. Hanamura (private communication).
[37] M. Steiner, in *Physics in One Dimension*, Proceedings of an International Conference, Fribourg, Switzerland, edited by J. Bernasconi and T. Schneider (Springer-Verlag, Berlin, 1981).